TRANSNAV
http://www.transnav.eu
the International Journal
on Marine Navigation
and Safety of Sea Transportation
Volume 14
Number 2
June 2020

DOI: 10.12716/1001.14.02.11

Reconstruction of Geomagnetic Event as Observed in Northern Adriatic Region and Its Correlation with GPS Single-frequency Positioning Deviations

D. Brčić, J. Ćelić & S. Valčić
University of Rijeka, Rijeka, Croatia

ABSTRACT: Space weather effects are generally recognized as causes of degradation of satellite positioning, navigation and timing (PNT) services. We analyze GPS position estimation error during a geomagnetic storm, focusing on manifestations of geomagnetic processes. The position estimation error was analyzed in terms of GPS coordinates' deviations (latitude, longitude and height) from their reference values. The storm's impact was studied in the Northern Adriatic region where GPS observables from two Global Navigation Satellite System (GNSS) reference stations were analysed. Geomagnetic indices were elaborated, comprising readings from interplanetary, magnetospheric and geomagnetic observatories. Total Electron Content (TEC) on both stations was computed using dual frequency GPS pseudorange observables. The experiment was to reconstruct the movement of geomagnetic disturbances entering the geospace, reaching the earth's surface. The aim was to correlate possible space weather manifestation on satellite positioning performance in terms of positioning error. Regularities in changes in positioning deviations were identified with relation to influential indices. The research offered a possibility of experimental positioning deviations assessment as well as forecasting. Evaluation of generated rudimentary Classification and Regression Trees (CART) models showed that the risk of satellite positioning errors could be assessed and predicted considering absolutes, as well as changes in values of geomagnetic indices. During the research process, several activities emerged as preferable continuation of the work, with the aim of further development of predictive models and the complement of space weather scenarios and their consequences on navigational systems. Along with summarized results, they are outlined in the conclusion section.

1 INTRODUCTION

The utilisation of PNT services is increasingly taking place in current and planned applications where high-precision and integrity of services are required. It reflects especially on critical applications in maritime navigation and transportation branches in general. Developing applications are requiring demanding tasks of sub-meter accuracy such as maritime operations, traffic management, search and rescue operations, marine engineering, as well as offshore and port systems operations. Furthermore, satellite positioning represents the primary navigational data source onboard vessels. The timing data accuracy is essential for the management of sailing passages, ports and approaches and navigational lights synchronisation (Thomas et al., 2011; Brčić, 2012). Performance degradation of GNSS services can affect certain system/application to a greater or lesser extent, depending on the level of required availability, integrity and accuracy (Thomas et al., 2011).

Satellite positioning performance is susceptible to errors caused by a number of individual causes,

varying from spatial distribution of satellites to user's micro-environment. Signal propagation error represents the main cause of single-frequency positioning degradation (Kintner and Ledvina, 2005; Parkinson and Spilker, Jr., 1996) with ionospheric delay as a prevalent positioning error cause (Klobuchar, 1983, 1987). Ionospheric delay is proportional to the amount of TEC on the path between the satellite and receiver antenna (Klobuchar, 1988). TEC is expressed in TEC Unit (TECU), one being 10^{16} e / m^2, equivalent to 1.624 meters of measured pseudorange error at GPS frequency L1 (Parkinson and Spilker, Jr., 1996).

TEC behavior varies depending on different occurrences and at different timescales (Mendillo, 2006); diurnal and seasonal variations, solar cycle and storm time behavior. The motivation of the conducted research was an attempt to create an image of near-earth space environment during disturbed space weather, before geomagnetic disturbances reach GNSS orbit heights, with eventual positioning deviations as final manifestation. A geomagnetic event was reconstructed to determine the relation between the geomagnetic storm effects and GPS positioning error. Data describing geomagnetic indices were analysed together with positioning observables on two International GNSS Service (IGS) stations in the Northern Adriatic area. Regularities of positioning patterns were detected as a response to the storm and variations in the geomagnetic field. Subsequently, the ionospheric analysis was made with local TEC behavior as a linkage between magnetic variations and the final positioning deviation. Event reconstruction was presented with the objective to confirm geomagnetic impact on satellite positioning performance. After analysed data interpretation, modeling of latitude, longitude and height deviations was introduced and evaluated. In the concluding chapter, research results and inferences were outlined along with planned activities which emerged from the research.

2 BACKGROUND

Satellite navigation technology presents an inevitable path towards improvements of transportation as a master link between sustainability pillars (Brčić, 2012). PNT services are used in all transportation branches, whether in traffic control management, monitoring or navigation. The European Union Single European Transport Area sub-projects are designed to ease the citizens and cargo movements and to enhance the European transport sustainability; however, the vision is global. Current and planned strategies imply an optimal infrastructure and reliable sources of dynamic information regarding PNT data provision (Thomas, 2011).

User Equivalent Range Error (UERE) encompasses influential quantities which are affecting time measurement of the satellite signal propagation, leading to erroneous pseudorange computation (Parkinson and Spilker, Jr., 1996; Subirana et al., 2013, Kaplan and Hegarty, 2006):

$$\rho = r + c \cdot \left(t_u - \delta t + \delta t_D \right) \quad (1)$$

where: ρ ... pseudorange between satellite and user antennae, r ... geometric (true) range between satellite and user antennae, t_u ... user clock error, δt ... satellite clock offset, δt_D ... the total ranging error generated by other influential factors.

The range measurement timing relations are shown in Figure 1, as interpreted from (Kaplan and Hegarty, 2006).

The ionospheric delay can be expressed as:

$$\Delta\rho = 40.3 / f \wedge 2TEC \quad (2)$$

where $\Delta\rho$ … equivalent ionospheric delay of determined pseudorange, f … system's operating frequency, TEC … Total Electron Content along an equivalent column between satellite and user's antenna with a cross section of 1 m^2.

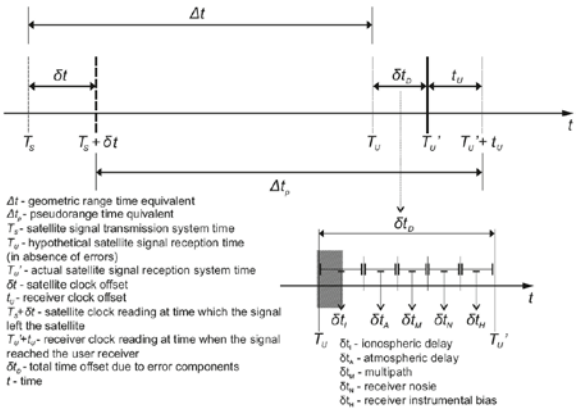

Figure 1. Range measurement timing relations

Influences on GPS positioning error during disturbed space weather have already been investigated in the area (Filjar et al., 2013), together with the development of GNSS positioning performance forecasting (Filić and Filjar 2018). Ionospheric disturbances are the consequence of changes, variations and occurrences resulting from conditions in the solar-terrestrial environment due to the manifestation of the solar activity (Parkinson and Spilker, Jr., 1996; Goodman, 2005). According to National Oceanic and Atmospheric Association's Space Weather Prediction Center (NOAA SWPC), geomagnetic storms, solar radiation storms and radio blackouts are described by numbered levels and with the corresponding indicators according to severity.

Geomagnetic activity is described by indices presented in Table 1 (Perrone and De Franceschi, 1998; Zolesi and Cander, 2014). Solar eruptive events create magnetic disturbances – Coronal Mass Ejections (CME) which travel through interplanetary space and interact with thermosphere, ionosphere and magnetosphere (Lockwood et al., 1999). The planetary Kp and Ap indices express the horizontal component of the geomagnetic stability. There appears a negative correlation between the *Kp* index and the storm-time TEC during summer months (Mendillo, 2006; Ross, 1960). The southward orientation of earth-directed interplanetary magnetic field (IMF) expressed with the *Bz* index causes the entering of power inputs in

the magnetosphere, producing geomagnetic disturbances (McMorrow, 2011).

Table 1. Geomagnetic indices

Index	Description
K/Kp	Three-hour pseudo-logarithmic index representing disturbances in horizontal component of the geomagnetic field in relation to quite space weather conditions.
Dst	One-hour indicator of magnetospheric activity, as a measure of the ring current in the magnetosphere. It can be interpreted as longitudinal average of horizontal geomagnetic disturbance.
AE	One-hour indicator of auroral (electrojet) activity, further divided in amplitude upper (*AU*) and amplitude lower (*AL*) indices with the relation *AE=AU-AL A/Ap* Linear equivalent of the *K/Kp* index, representing average of geomagnetic field variations
aa	Global geomagnetic activity index derived from two mutually antipodal magnetic observatories.
BT	Geomagnetic field intensity indicator, which can be further decomposed into northing, easting and vertical component.

The *Bz* index is one of the first qualitative storm indicators, as its southward pointing triggers processes in the geospace, including an opening of the magnetosphere (Lockwood et al., 1999). The magnetospheric opening causes increased ring current (*Dst*), allowing the energy and particles to enter through auroral ovals (*AE*/*AU*/*AL*) and spread over the globe (Mendillo, 2006; Booker, 1954). These processes lead to disturbances in the ionospheric F2 region and on distribution and behavior of the total electron content (Davies, 1965).

3 METHODOLOGY

The first group of analysed parameters refers to geomagnetic indices, while the second represents three-dimensional satellite positioning deviations obtained with GPS. Readings of magnetic field changes in the magnetosphere were retrieved from the Geostationary Operational Environmental Satellite (GOES) 15 measurements archive (Singer et al., 1996). Apart from geostationary observations, readings of magnetospheric field components were retrieved from Advanced Composition Explorer (ACE) spacecraft observables, measured at Libration 1 point.

Earth observations were analysed near to the Northern Adriatic region, using nearest of International Real-Time Magnetic Observatory Network (INTERMAGNET) observatories (Chambon la Foret, France). Global geomagnetic indices *Dst*, *AE*, *AU*, *AL* and *Kp,* were retrieved from the World Data Center for Geomagnetism (WDC) and Space Physics Interactive Data Resource (SPIDR) databases. Collection, processing, determination and creation of GPS positioning solutions were enabled using Reader Independent Exchange Format (RINEX) databases, available at International GNSS Service and US NGS CORS servers (Gurtner and Estey, 2009). Data from two stations were analysed: Bolzano, Italy and Graz, Austria (Table 2). It is assumed that the consistency and quality of IGS data is ensured through (Kouba, 2009), focusing on the removal of non-dispersive pseudorange error components, such as multipath (< 0.3 m), cycle slips (< 1 per 1000 observations), northing, easting and height eccentricities to the antenna reference point (≤1 mm), and other requirements needed for the provision of high-quality and high-integrity GNSS products.

Table 2. General information of Bolzano and Graz IGS stations

ID	City	Location	Longitude (E)	Latitude (N)	Height (m)
bzrg	Bolzano	Italy	11.3368	46.4990	328.8
graz	Graz	Austria	15.4935	47.0671	538.3

GPS positioning files (RINEX.pos) were calculated and archived using RTKLIB open source program package, employing observation and navigation files. The ionospheric correction was settled by employing standard ionospheric model, coefficients of which were taken from diurnal navigational messages. Other standard methods and algorithms were settled as follows: single positioning mode, L1 frequency (single) positioning solution, 15° elevation mask, broadcast ephemeris, continuous ambiguity resolution and tropospheric model (Saastamonien). Ionospheric TEC was calculated by using dual-frequency (L1 and L2) GPS measurements from IGS stations. Measured phase differences (TEC_ϕ) were smoothed with code differences (TEC_P), after which they were leveled again using code differences to correct TEC values (Dyrud et al. 2008):

$$TEC_P = \frac{P_2 - P_1}{0.104 m TECU^{-1}} \tag{3}$$

$$TEC_\phi = \frac{\phi_1 - \phi_2}{0.104 m TECU^{-1}} \tag{4}$$

After Differential Code Biases (DCB) correction (Noll, 2010), it is assumed that all frequency-dependent quantities except ionospheric delay were eliminated (Subirana et al., 2013). Standard deviations of computed values were presented as well. The total electron content was derived using *GPS-TEC* software from IGS stations' RINEX files, by using described mathematical relations.

Time series were analyzed from all parameters, along with statistical summaries and distribution of collected data. The event phases were further divided, isolating specific influences and different behavior of indices (e.g. depletion and enhancement of TEC). Correlation between variables was made using Pearson's correlation coefficients for the two most pronounced observed events.

Recursive binary splitting (partitioning) algorithm was used to develop a decision tree model, which the main objective is to minimise the Residual Sum of Squares (RSS) given as (Hastie et al., 2009):

$$RSS = \sum_{m=1}^{M} \sum_{i \in R_m} \left(y_i - \hat{y} R_m \right)^2 \quad (5)$$

where: M ... partitions of partitioned feature space, y_i ... response of a particular testing observation, and $\hat{y} R_m$ ... mean response of the training observation within partition m.

Development of such models is based on the concept of splitting the observed data set into subsets and on the values of predictors in a series of iterations (Filić and Filjar, 2018).

For the sake of simplicity, the procedure was limited to the determined depth of a tree. The general model is given as follows (Hastie et al., 2009, James et al., 2013):

$$f(\mathbf{x}) = \mathbb{E}(y|\mathbf{x}) = \sum_{m=1}^{M} w_m \phi(\mathbf{x}; \boldsymbol{\nu}_m) \quad (6)$$

where: w_m ... the mean response for the particular region R_m, and ν_m represents how each variable is split at a particular threshold value.

During splitting, *Gini index* as the main criteria was used to assess the function (Hastie et al., 2009, James et al., 2013):

$$i(t) = 1 - \sum_{j=1}^{k} p^2(j|t) \quad (7)$$

where: k ... the number of possible output categories, while the category j has a probability of occurrence $p(j|t)$.

After several algorithm repetitions, the final selection of indices was made, also considering the correlation results. Regression trees as predictive models were generated for each positioning component as target variables. The final output of models was the estimation of probable values of latitude, longitude and height deviations, respectively. Proposed models were evaluated employing observed and predicted values. Partitioning of used data-sets was divided as 70% for training, 15% for validation and 15% for evaluation, respectively.

4 THE EVENT

In this section, the geomagnetic event was described, as occurred through June 21 – 27, 2015 following official event reports, using available data and followed with own interpretation.

4.1 *Geomagnetic storm development*

According to the United States Geological Survey (USGS) National Geomagnetism report, the storm occurred because of solar wind fast stream and CMEs, arriving on June 21st at 16:45 UT (day of year (DOY) 172), June 22nd at 05:45 UT (DOY 173), and June 22nd at 18:30 UT, compressing the magnetosphere and generating electric currents and geomagnetic field perturbations.

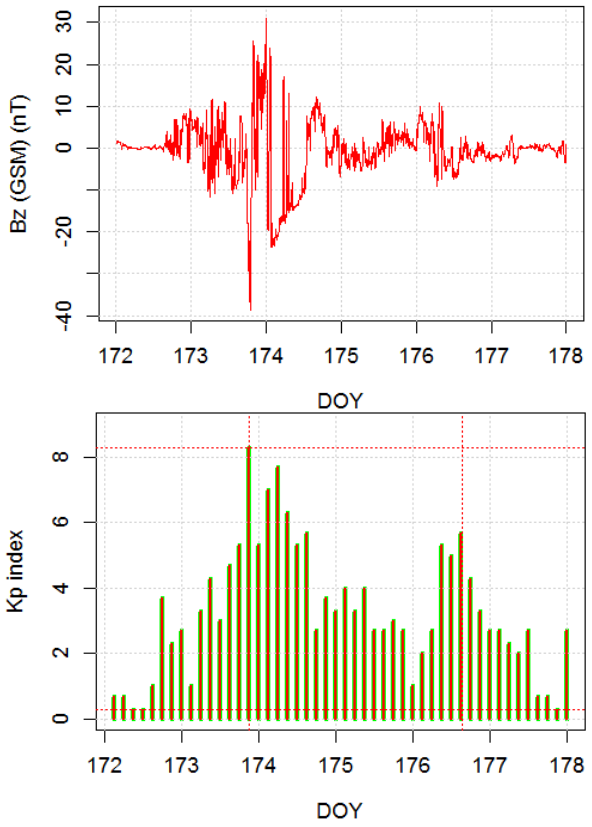

Figure 2. IMF Bz component magnitude 4-minue level data (top) and Kp index (bottom) 3-hours data through the storm period, DOY 172-177

In a specific moment, IMF *Bz* component turned southward (Figure 2). Geomagnetic activity arose firstly at high latitudes, as shown in Figure 3. The greatest *Dst* depression occurred on June 23rd at 04:30 UT and recovering until another CME reached the earth (Figure 3). The sub-events formed geomagnetic storm period of seven days. Statistical parameters were calculated based on the time series for the specific indices, as presented in Table 3.

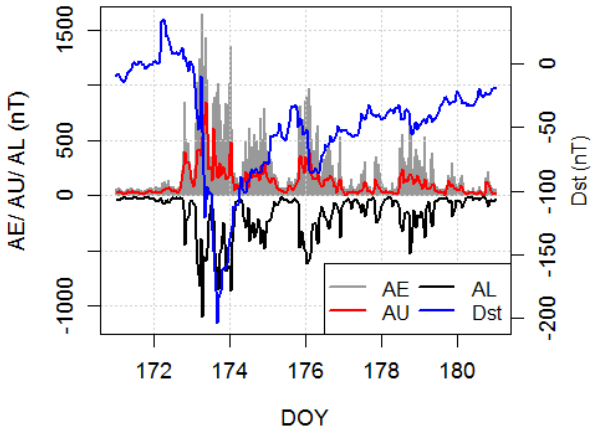

Figure 3. Auroral activity and Dst values, DOY 171 – 181

According to (Singer et al., 1996), nominal (undisturbed) total geomagnetic field intensity (*BT*) measured on satellite vary from -200 nT to +200 nT. The *BT* maximum value and range exceeds the limits several times.

Table 3. Statistical description of geomagnetic indices during DOY 172-177

Index	Min	Mean	SD	Max	Range
GOES *BT* (nT)	33.93	139.5135	72.2918	1,289.21	1,255.28
Dst (nT)	-204.00	-46.34	41.2002	836.00	-240
AE (nT)	31.00	280.30	296.56	781,636.00	1,605
AU (nT)	6.0	115.7	123.0969	841.0	835
AL (nT)	-1,101.0	-164.6	190.7277	-13.0	1,088
Kp	0.300	3.273	8.300	1.9665	8.0
CLF *BT* (nT)	47,741.3	47,824.5	25.6576	47,976.3	234.96

Pronounced values indicate geomagnetic storm and travelling disturbances and high variations. The *Kp* increased two times; the maximum of 8.3 took place just before the commencement of day 174 (June 23rd), associated with June 21st and June 22nd CMEs. The second increase occurred on day 176 (June 25th) after another solar eruption and CME arrival, respectively.

4.2 *Storm-time GPS positioning deviations*

Time series of deviations of positioning components were calculated for the period June 22nd (DOY 173) – June 26th UTC (DOY 177). Horizontal deviation plots are shown in Figure 4.

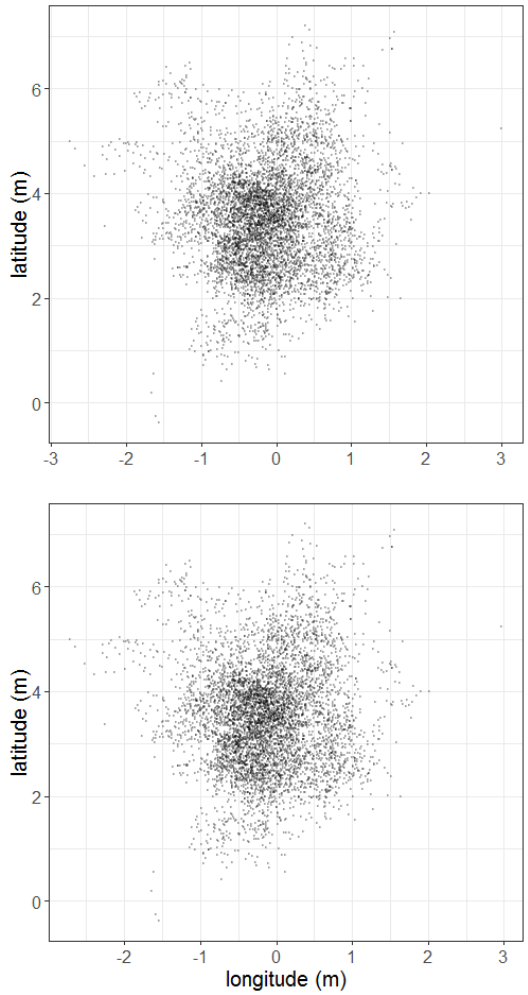

Figure 4. Horizontal positioning error as calculated for stations Bolzano (top) and Graz (bottom).

Statistical description of GPS positioning error through the observed period is shown in Table 4, with arc units converted to meters.

Table 4. Bolzano (B) and Graz (G) horizontal positioning error during the storm period

Station	Lat error (m)		Long error (m)		Height error (m)	
	Mean	SD	Mean	SD	Mean	SD
G	4.191	1.017	-1.350	0.546	1.572	1.849
B	3.524	1.028	-0.126	0.6	0.098	1.875

The distribution of observed height values for both stations is presented in Figure 5.

Although there is a constant offset relative to reference values, latitude and longitude are experiencing smaller deviations when compared to height, tending northward (latitude) and eastward (longitude), respectively. Standard deviations are approximately the same at both locations and in all axes; however, vertical component shows the most prominent scattering.

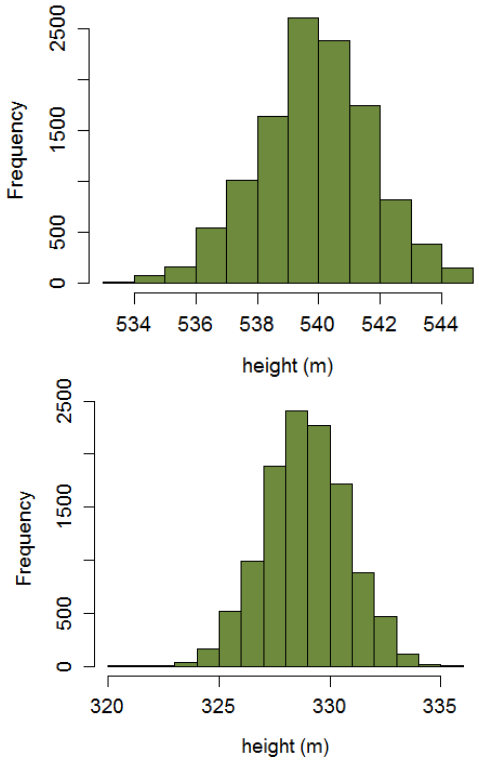

Figure 5. Height histograms for Graz (top) and Bolzano (bottom)

Statistical description of daily positioning deviations is graphically presented in Figure 6, showing minimal and maximal values and range, mean values and standard deviation, respectively.

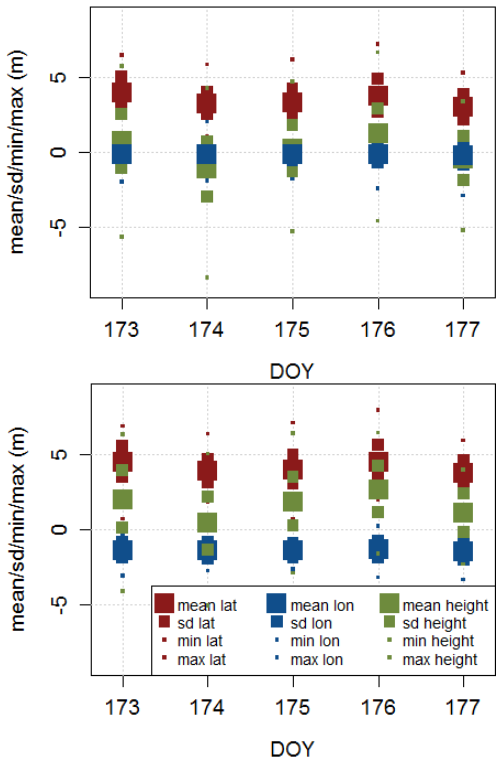

Figure 6. Bolzano (top) and Graz (bottom) daily horizontal positioning error statistics

4.3 *Interpretation of results*

The TEC patterns during the storm period with computed mean values and standard deviations are shown in Figure 7.

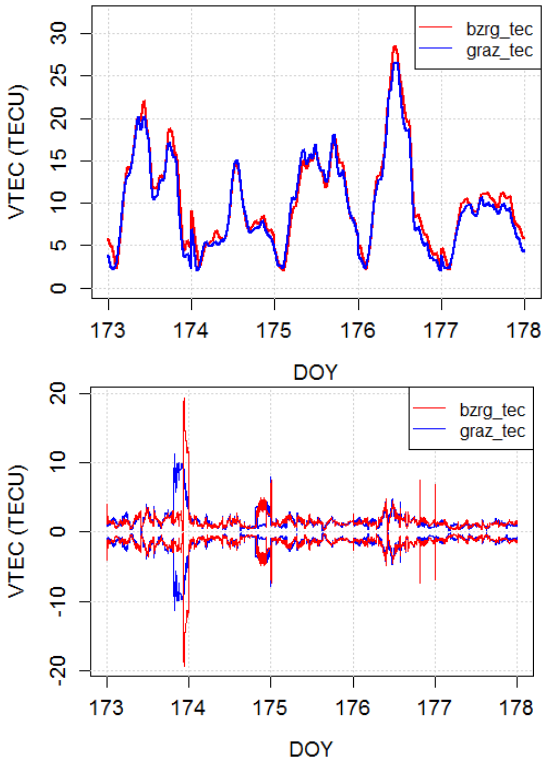

Figure 7. TEC daily patterns mean values (top) and standard deviations (bottom) as computed for locations Bolzano and Graz during the storm period

In Table 5, statistical parameters of the computed storm-time period TEC at locations Bolzano and Graz are presented.

Table 5. Statistical description of the total electron content

Station	Minimum value	Mean value	Standard deviation	Maximum value	Range
Bolzano	2.09	10.36	5.59	28.55	26.46
Graz	2.03	9.78	5.51	26.57	24.54

On Figure 8, readings from GOES magnetometers 1 and 2 are presented, together with geomagnetic field intensity as measured on Chambon-La-Foret observatory. On Figure 9, combined plots of positioning error deviations for Bolzano and Graz locations are shown, together with associated TEC computed on both locations. The illustrations are followed with interpreted results.

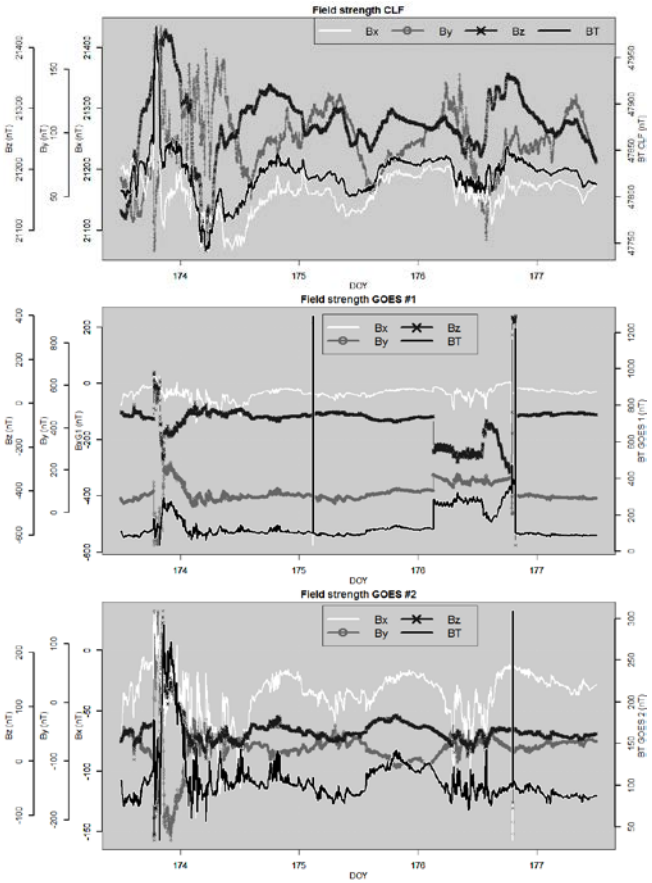

Figure 8. Geomagnetic field intensity as measured with Chambon-La-Foret (top), GOES 1 (middle) and GOES 2 (bottom) magnetometer

Abrupt change (depression) of TEC (DOY 173) preceded the increase of geomagnetic field intensity. After geomagnetic peak values and during TEC decline (end of DOY 173 / beginning of DOY 174), positioning deviations were most pronounced. At the same time, the greatest *Dst* drop and *AE* increase occurred. During first hours of day 174, a measurable TEC peak occurred.

TEC commotions accompanied the second positioning deviations increase on DOY 174. During DOY 175, all the observed values were returning in regular patterns. The increase of *Dst* indicated

possible commencement of new geomagnetic disturbance.

The DOY 176 is characterized by *Dst* decline, an increase of auroral activity and stirrings of all (magnetospheric and ground) magnetic field components. Total geomagnetic field flux measured at GOES magnetometer 1 reached the greatest value during this period. Second GOES magnetometer shows oscillations of magnetic components around the mean values, like ground readings. The drop of *Bz* component as measured on the first GOES magnetometer is here pronounced. Positional deviations started to increase, reaching maximum values before midday. The following hours were characterised with TEC increase, reaching its greatest observed values. The magnetospheric total field strength was the highest observed.

The disturbance ceased the following day, which can be interpreted from regular patterns of geomagnetic components, as well as TEC lowering. In line with described patterns, positioning deviations are also decreasing, returning to normal values.

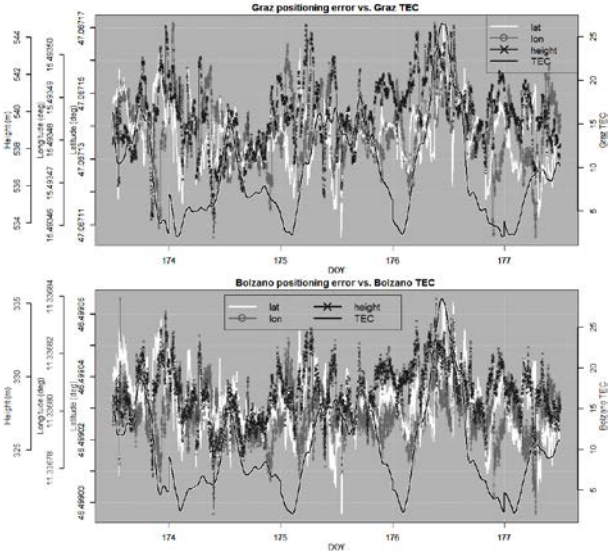

Figure 9. Graz (top) and Bolzano (bottom) latitude (red), longitude (blue) and height (green) positioning deviation patterns, with total electron content (black), computed at each location

5 DISCUSSION

Two distinctive incidents (events) can be extracted: abrupt depression and subsequent rise on DOY 173 and pronounced increase on DOY 176.

For these two periods geomagnetic, positioning and TEC parameters were used to find mutual correlations. The results are shown in Figure 10 and in Figure 11. During the first event, the total magnetic field intensity measured on all magnetometers (*BTCLF*, *BTG1* and *BTG2*) correlated positively with latitude and height positioning errors (*bzrg_fi*, *bzrg_h*, *graz_fi*, *graz_h*), while negative correlation were found with longitude errors (*bzrg_l*, *graz_l*). The TEC (*bzrgtec*, *graztec*) showed negative correlations with components of GOES-measured geomagnetic activity, and positive correlation with ground-based magnetic readings. During the second event, *BTG1* showed a positive correlation with positioning components, opposite to Chambon-La-Foret (ground) readings, same being applicable for TEC.

Positioning deviations were most expressed during pronounced changes in geomagnetic field intensity components, measured with GOES magnetometer 1 (*BxG1*, *ByG1*, *BzG1*, *BTG1*), GOES magnetometer 2 (*BxG2*, *ByG2*, *BzG2*, *BTG2*) and Chambon-La-Foret (*BxCLF*, *ByCLF*, *BzCLF*, *BTCLF*). The TEC behavior showed correlation with geomagnetic activity and the affectation of the geomagnetic impact on both stations similarly.

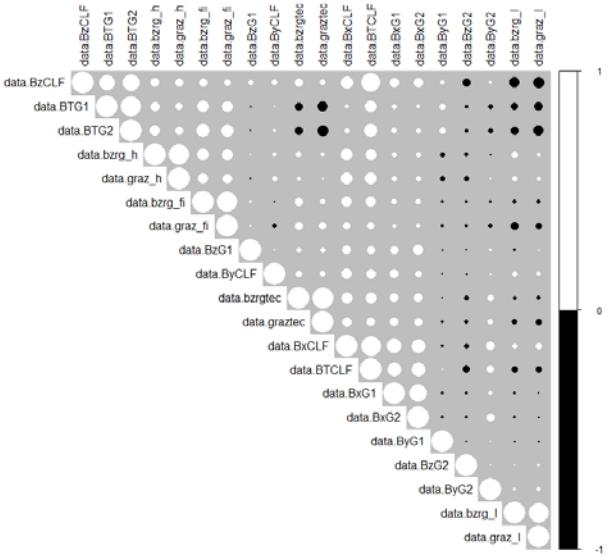

Figure 10. Correlation matrix between variables during the first event. The dots size indicates positive (white) or negative (black) correlation.

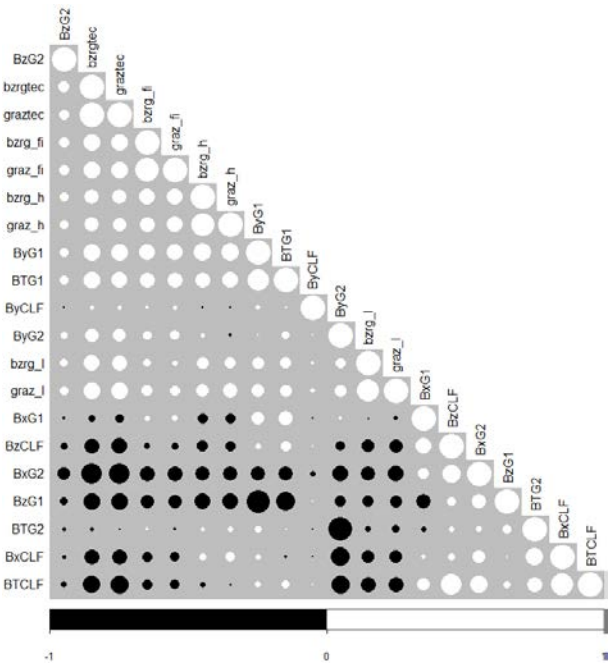

Figure 11. Correlation matrix between variables during the second event. The dots size indicates positive (white) or negative (black) correlation.

The time of commencement and duration of the main phase of the storm (DOY 173.5 – 174.5) was extracted for modeling of positioning deviations of

components on station Graz: latitude (*devFIG*), longitude (*devLG*) and height (*devHG*). During the height model-building process, main components were defined as *AU, BTCLF, BxCLF, BzCLF, BzG1, TEC, dTEC,* and *Dst*. A similar process was made for latitude and longitude models, respectively. Governing indices were found as follows:

– Latitude model: AE, AL, ByCLF, ByG1, ByG2, dBzCLF, TEC, Dst,
– Longitude model: AE, AU, BTG1, BTG2, ByCLF, ByG1, BzCLF, TEC, Dst.

For the latitude target variable, the root node was a northing magnetic component as measured on second GOES magnetometer (*ByG2*), while the total magnetic field intensity (*BTG1*) was the root node for the longitude model.

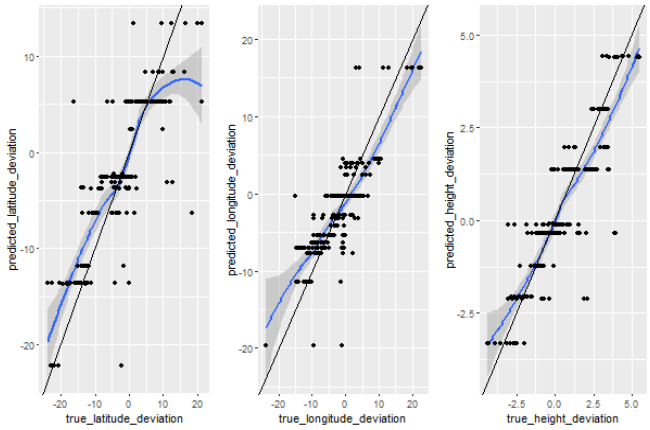

Figure 12. Latitude (left), longitude (centre) and height (right) deviations model evaluation

Decision tree models can develop certain drawbacks in the form of extreme sensitivity and ease of over-fitting. However, they represent a simple decision-making tool. The success of models will depend on the appropriate selection of possibly influential quantities. As for the proposed models, obtained results were compared with observed values of positioning deviations. Evaluation of models is shown in Figure 12. The plots are showing observed versus predicted values, local regression scatterplot smoothing, regression lines and confidence intervals.

Considering adjusted R-squared, the average overall score of the efficiency of models is 71.4% (Table 6).

The height model showed the best performance (78%). In general, vertical satellite positioning component is most susceptible to external influences. The latitude model evaluation results showed 69%, and longitude model showed 67% of performance efficiency, respectively.

Table 6. Model evaluation output: observed against predicted values regression analysis

Height deviation model			
Coefficients	Estimated coefficient	Standard Error	Pr(>|t|)
Intercept	0.19438	0.06719	0.00421
Predicted deviation	0.96744	0.03458	< 2e-16
R-squared	Multiple: 0.7845	Adjusted: 0.7835	
F-statistic: 782.5 on 1 and 215 DF	p-value: < 2.2e-16		
Latitude deviation model			
Coefficients	Estimated coefficient	Standard Error	Pr(>|t|)
Intercept	-0.1192	0.3568	0.739
Predicted deviation	0.9921	0.04552	< 2e-16
R-squared	Multiple: 0.6884	Adjusted:0.687	
F-statistic: 475 on 1 and 215 DF	p-value: < 2.2e-16		
Longitude deviation model			
Coefficients	Estimated coefficient	Standard Error	Pr(>|t|)
Intercept	-0.1277	0.28384	0.653
Predicted deviation	0.9274	0.04413	< 2e-16
R-squared	Multiple:0.6726	Adjusted:0.6711	
F-statistic: 441.7 on 1 and 215 DF	p-value: < 2.2e-16		

6 CONCLUSIONS

The amount and intensity of space weather effects on PNT services depend on an individual event. A geomagnetic event which took place in June 2015 was studied in this paper. The initial aim was the reconstruction of the flow of geomagnetic occurrences from magnetospheric heights up to the surface of the earth, and to correlate geomagnetic indices with the GPS positioning deviations. The storm period was fragmented in sub-events, each characterised with specific behavior of indices. Data interpretation and subsequent analysis showed that positioning deviations followed changes in geomagnetic field intensity. Ionospheric TEC was introduced as an entity which complemented the storm features and its manifestation on positioning. Characteristic changes in TEC behavior during times of geomagnetic variations were observed. After the correlation between all employed variables, regression tree models were introduced to determine probable values of positioning deviations as target variables. The evaluation of models showed an acceptable level of success, especially reflecting on height deviation prediction as the most sensitive positioning component. The proposed approach offers a simple yet effective mean of assessment of GPS positioning performance during space weather events directly or indirectly affecting positioning deviations.

The storm was not classified as extreme; however, it measurably influenced the positioning performance. With ever growing GNSS utilisation, such events could affect the simultaneous performance of GNSS-based services that are expected to be independent of each other. Further research of similar events and employment of additional indices is necessary to contribute to a more comprehensive image of the solar-terrestrial environment. Besides geomagnetic disturbances, models should also employ solar, solar wind and ionospheric indices, opening possibilities of predictive

analytics by monitoring upcoming disturbances from their place of origin.

ACKNOWLEDGMENTS

This work has been fully supported by the University of Rijeka under the project – *uniri-tehnic 18-66*. The authors would like to thank N. Ness, Principal Investigator of Bartol Research Institute and to Dr. Howard Singer, NOAA Chief Scientist. Authors appreciate and support the access to open software tools: R, R Studio and Rattle, RTKLIB and Rinex-GPS-TEC.

REFERENCES

Booker, H.G., Morphology of Ionospheric Storms, *Proceedings of the National Academy of Science of the United States of America*, PNAS, Washington DC, 1954, vol. 40, no. 10, pp. 931–943.

Brčić, D., Ensuring sustainability through utilisation of satellite navigation technology, *Proceedings of the 2012 International Conference on Transport Sciences (ICTS)*; Portoroz, Slovenia, Fakulteta za pomorstvo in promet, 2012, p 14.

Davies, K., *Ionospheric Radio Propagation*, National Bureau of Standards, Washington DC, 1965.

Dyrud, L. et al., Ionospheric measurement with GPS: Receiver techniques and methods. *Radio Science*, 2008, vol. 43, no. 6, pp. 1-11.

Filić, M. and Filjar, R., *Forecasting model of space weather-driven GNSS positioning performance*. Lambert Academic Publishing, Saarbrucken, 2018.

Filjar, R., Brčić, D. and Kos, S., Single-frequency Horizontal GPS Positioning Error response to a moderate Ionospheric storm over Northern Adriatic, In: Weintrit, A. (ed) *Advances in Marine Navigation*, *Marine Navigation and Safety of Sea Transportation*, CRC Press, Boca Raton, 2013, pp. 49-56.

Goodman, J.M., *Space Weather and Telecommunications,* Springer, New York, 2005.

Gurtner, W. and Estey, L., *RINEX: The Receiver Independent Exchange Format, V3.01*, IGS Central Bureau, Pasadena, 2009, p. 44.

Hastie. T., Tibshirani, R. and Friedman, J., *The Elements of Statistical Learning*, Springer, New York, 2009.

James, G., Witten, D., Hastie, T. and Tibshirani, R., *An Introduction to Statistical Learning*, Springer, New York, 2009.

Kaplan, E.D. and Hegarty, C.J., *Understanding GPS: Principles and Application*, 2nd ed., Artech House, Boston, 2006.

Kintner, P.M. and Ledvina, B., The ionosphere, radio navigation and global navigation satellite systems, *Advances in Space Research*, 2005, vol 35, no. 5, pp. 788-811.

Klobuchar, J.A., Ionospheric corrections for timing applications, *Proceedings of the 20th Annual Precise Time and Time Interval (PTTI) Application and Planning Meeting*, Naval Observatory, Washington DC, 1988, pp. 193-201.

Klobuchar, J.A., *Ionospheric Effects on Earth-Space Propagation*, Environmental research paper No. 866, Air Force Geophysics Laboratory, Hanscom, 1983, p 33.

Klobuchar, J.A., Ionospheric Time-Delay Algorithm for Single-Frequency GPS Users, *IEEE Transactions on Aerospace and Electronic Systems*, 1987, vol. 23, no.3, pp. 325–331.

Kouba, J.A., *Guide to using International GNSS Service (IGS) products*, IGS Central Bureau, Pasadena, 2009, p. 34.

Lockwood, M., Wild, M.N., Stamper, R., Davis, C.J. and Grande, M., Predicting Solar Disturbance Effects on Navigation Systems, *Journal of Navigation*, 1999, vol. 52, no. 2, pp. 203-216.

McMorrow, D., *Impacts of Severe Space Weather on the Electric Grid*, Report JSR-11-320, The MITRE Corporation, McLean, 2011, p. 107.

Mendillo, M., Storms in the ionosphere: Patterns and processes for total electron content, *Reviews of Geophysics*, 2006, vol. 44, no. 4, p. 47.

Noll, C., The Crustal Dynamics Data Information System: A resource to support scientific analysis using space geodesy, *Advances in Space Research*, 2010, vol. 45, no. 12, pp. 1421-1440.

Parkinson, B.W. and Spilker, Jr. J.J., *Global Positioning System: Theory and Applications*, Vol. I, AIAA, Washington DC, 1996.

Perrone, L. and De Franceschi, G., Solar, ionospheric and geomagnetic indices, *Annals of Geophysics*, 1998, vol. 41, no. 5-6, pp. 843-855.

Ross, W.J., The determination of ionospheric electron content from satellite Doppler measurements: 2, Experimental results, *Journal of Geophysical Research*, 1960, vol. 65, pp. 2607–2615.

Singer, H.J., Matheson, L., Grubb, R., Newman, A. and Bouwer, S.D., Monitoring space weather with the GOES magnetometers, *Proc. SPIE 2812, GOES-8 and Beyond*, 1996, p. 29.

Subirana, J. S., Zornoza, J. M. J. and Hernandez-Pajares, M., *GNSS Data processing, Volume I: Fundamentals and algorithms*, ESA Communications, Noordwijk, 2013.

Thomas, M. et al., *Global Navigation Space Systems: reliance and vulnerabilities*, RAENG, London, 2011.

Zolesi, B. and Cander, R. L. J, *Ionospheric Prediction and Forecasting*, Springer, New York, 2014.